Journal of Industrial and Engineering Chemistry 59 (2018) 134–140

Contents lists available at ScienceDirect

Journal of Industrial and Engineering Chemistry

journal homepage: www.elsevier.com/locate/jiec

Cu/Al and Cu/Cr based layered double hydroxide nanoparticles as adsorption materials for water treatment

Stefan Berner, Paulo Araya, Joseph Govan, Humberto Palza*

Departamento de Ingeniería Química y Biotecnología, Facultad de Ciencias Físicas y Matemáticas, Universidad de Chile, Santiago, Chile

ARTICLE INFO

Article history:
Received 28 August 2017
Received in revised form 3 October 2017
Accepted 6 October 2017
Available online 14 October 2017

Keywords:
Layered double hydroxides
Adsorption
Layered double oxides

ABSTRACT

Cu/Al and Cu/Cr layered double hydroxides (LDH) were synthesized using a simple co-precipitation method at room temperature. These particles were further modified by Co^{+2} incorporation, and calcined at 500 °C for synthesis of layered double oxides (LDO). The LDH crystallinity or these samples highly depended on the composition, with Cu/Al-LDH presenting much higher order than Cu/Cr-LDH. High values of methyl orange adsorption were measured especially after calcination. For instance, Cu/Al and Cu/Co/Al LDH exhibited maximum monolayer adsorption capacities of 313 and 240 mg/g, respectively, meanwhile the same particles transformed into LDO presented values of 780 and 583 mg/g.

Introduction

The presence of organic pollutants in water represents an important environmental concern as they can turn this element into an unusable resource. Dyes in particular, mainly used in the textile industry, are known as one of the most worrying water contaminant because conventional water treatment plants cannot deal with them efficiently [1,2]. In order to treat this kind of contaminant, different mechanisms have been tested such as oxidation, filtration, photocatalysis, adsorption, coagulation, and ozonation, among others [3–5]. In this context, layered double hydroxide particles (LDH) show as good a performance in removal of pollutants as in photocatalysis [6].

LDH are a type of anionic clays having a hydrotalcite crystal structure, that are formed by two kinds of metal ion, usually a divalent and a trivalent one, together with hydroxyl groups, an interlayer anion, and water molecules. LDH are formed following the general formula $\left[M_{1-x}{}^{+2}M_x{}^{+3}(OH_2)\right]^{+x}\left[A_{x/n}\right]^{-n}\cdot mH_2O$, where x is the molar ratio $M^{+3}/\left(M^{+2}+M^{+3}\right)$, ranging from 0.20 to 0.33 in order to avoid the formation of undesirable phases [7]. The presence of different metals in the LDH structure can confer semiconductor character associated with an energy gap between the valence and the conduction band. In this way, several types of LDH have been produced showing a photo-induced electron transition suitable for photocatalysis treatment of polluted water by advanced oxidative reactions [8]. For instance, Zn/Ti LDH presented a low band gap of 3.1 eV exhibiting significant photo-catalytic activity for the degradation of methylene blue under visible light irradiation [9]. Moreover, Ni/Co/Ti LDH has been recently synthesized by a single step hydrothermal route exhibiting photodegradation of both cationic and anionic dyes [10]. From the different divalent metals used, copper is notable due to its outstanding photocatalytic behaviour enabling the electrons being excited by visible light and therefore increasing photo-catalytic activity by a reduction in the energy gap [11]. Tian et al. synthesized Cu/Cr LDH immobilized on a copper substrate by electrophoretic deposition which showed excellent photocatalytic activity for the degradation of organic pollutants due to broad adsorption bands in the visible region [12]. Parida et al. produced Cu/Cr LDH for degradation of malachite green showing that the incorporation of cobalt atoms increased the photocatalytic activity depending on the Cu/Co molar ratio [13]. The band gap found in these Cu/Cr LDH ranged from 1.73 to 2.43 eV, depending on the composition explaining partially the high photodegradation observed. Copper was also used as substitute ion in Zn/Al LDH improving, for instance, the photocatalytic behaviour toward degradation of orange II [14]. By increasing the amount of copper,

* Corresponding author.
E-mail address: hpalza@ing.uchile.cl (H. Palza).

https://doi.org/10.1016/j.jiec.2017.10.016
1226-086X/

the photocatalytic degradation of 2,4,6-trichlorophenol under visible light was improved as concluded by testing several LDH based materials with different organic/inorganic Cu species [15].

Another characteristic of LDH regarding water treatment is their high adsorption capacity, especially toward anionic dyes [6]. This adsorption arises from anion exchange reactions between the counter-ion and the anionic dye producing a distortion on the interlayer distance because of the different size of the anions [16]. For instance, Lu et al. prepared Mg/Al LDH for Congo red adsorption using magnetic microparticles for a removal mechanism [17]. Another Mg/Al LDH was synthetized by a hydrothermal route at 100 °C obtaining a well-crystallized material with an adsorption capacity of 148 mg/g over methyl orange (MO) [18]. Copper based LDH also showed adsorption capacity of dyes and Cu/Al LDH was able to treat methyl violet 2B achieving a maximum adsorption capacity of 361 mg/g [19]. By changing the intercalated carbonate ions for organic molecules, Kameda et al. produced Cu/Al LDH able to remove phenol derived molecules [20]. Recently, great interest has been shown for the use of LDH for coagulation of carbon based nanoparticles such as graphene oxide (GO) and carbon dots [21–23]. The coagulation process arises from electrostatic interactions and hydrogen bonds between GO and the abundant oxygen-containing functional groups on LDH surfaces. In this way, nanoparticles can coagulate on the LDH surface [24].

A strategy to improve adsorption process in LDH is their calcination obtaining layered double oxides (LDO) that can be re-transformed to LDH in aqueous solution [25]. For instance, Mg/Al LDH having Ni atoms calcined and aged at 65 °C, achieved an MO adsorption capacity of 375 mg/g [26]. Yao et al. calcined a glycerol-modified Mg/Al LDH prepared by hydrothermal method achieving a maximum adsorption capacity of 1062 mg/g over MO [27]. Notably, Lei et al. recently reached 1250 mg/g of adsorption capacity for Congo red with a Ni/Al LDH having Mg atoms [28]. Regarding calcined Cu-based LDH, most research has been concentrated on the catalytic performance of the material without any focus on adsorption [29–34].

Despite the above mentioned good results regarding LDH for water treatment, most of the methods applied for their synthesis are highly energy intensive due to the complex processes used, like hydrothermal syntheses. Moreover, for adsorption studies based on LDO, copper based particles had not been reported. Herein, we synthesized a set of copper based LDH by a simple co-precipitation method at room temperature for adsorption of MO, that were further calcined to obtain copper based LDO nanoparticles. By this simple method, copper based LDH materials were synthesized overcoming partially the Jahn–Teller effect of Cu^{2+} ions that produces distortions into their octahedral structures forming precipitated by-products [35–37]. Copper was selected as M^{+2} for LDH/LDO materials due to its great versatility allowing the development of multifunctional materials with several applications such as in catalyst, adsorption, antimicrobial compounds, and energy storage [38,39]. Although Al is the most studied M^{+3} ions in these copper based LDH, we also studied Cr due to potential photocatalytic enhancement [12,13].

Experimental parts

Materials

Copper nitrate ($Cu(NO_3)_2{\cdot}3H_2O$), Aluminum nitrate ($Al(NO_3)_3{\cdot}9H_2O$), Cobalt nitrate ($Co(NO_3)_2{\cdot}6H_2O$), Chromium nitrate ($Cr(NO_3)_3{\cdot}9H_2O$), Sodium carbonate (Na_2CO_3) and methyl orange (MO) were purchased from Sigma Aldrich and Sodium hydroxide (NaOH) from Merck. All these reagents were used without further purification. Distilled water was used as solvent.

Synthesis of LDH and LDO

A typical co-precipitation method was used to get Cu/Al and [CuCo]/Al LDH, labelled as CA and CCA, respectively. For CA LDH, a 50 mL of water solution containing Copper nitrate, Aluminum nitrate, and another 50 mL water solution containing 1.25 g of NaOH, were simultaneously added dropwise into a third solution of 100 mL of water containing 0.58 g of Na_2CO_3 at room temperature. The values of metal nitrate compounds were changed to obtain a molar ratio of: 3:1; 5:2; and 2:1. The pH was fixed at 10 by controlling the flow of each solution. Afterward, the solution was vigorously stirred for 6 h, and left overnight at room temperature with no stirring. Finally, the supernatant was taken and the sediment was redispersed in water and repeatedly centrifuged until the supernatant's pH was close to 7. For CCA synthesis, the procedure was the same, but the first solution was prepared by adding 2.00 g of Copper nitrate, 0.82 g of Cobalt nitrate and 1.67 g of Aluminum nitrate into 50 mL of water.

Chromium based LDH were synthetized by the same route although changing the quantities of the first solution. For Cu/Cr (labelled CC), 2.52 g of Copper nitrate and 2.08 g of Chromium nitrate was used while for [CuCo]/Cr (labelled CCC) 0.63 g of Copper nitrate, 2.28 g of Cobalt nitrate and 2.08 g of Chromium nitrate was used. The ratio between the M^{II} and M^{III} metal cations was unchanged.

For LDOs, a certain amount of each LDH was calcined at 500 °C for 4 h using a 15 °C/min temperature gradient and labelled as CA500, CCA500, CC500 and CCC500.

Characterization

LDH crystalline structure was analyzed by XRD which was recorded with a D8 Advanced Bruker diffractometer using Cu Kα radiation (λ = 1.5418 Å). The morphology of LDH and LDOs were observed using scanning electron microscopy (SEM) FEI-Inspect F50 between 10 and 20 kV. Determination of the specific surface area of the catalysts was made measuring N_2 adsorption in a Micromeritics sorptometer, Model ASAP 2010. The samples were previously degassed at 200 °C. The UV–vis DR analyses were made on a Perkin Elmer Lambda 650 instrument equipped with a Praying Mantis and a Harrick powder cell.

Adsorption experiments

For the maximum adsorption capacity over MO, 3 mg of each sample (CA, CCA, CA500 and CCA500) were added into four 15 mL Falcon tubes containing 10 mL of MO solution with concentrations ranging from 50 to 200 mg/L for LDH and 150 to 300 mg/L for LDO. The tubes were shaken for 24 h and centrifuged afterwards. A small sample was taken from each tube and its MO concentration was calculated as it was made for the photocatalytic tests. The Langmuir and Freundlich models were used to obtain the main parameters related with the equilibrium adsorption as below explained.

Recycling capacity

To determine how the material works after several cycles of adsorption, the CCA500 sample was tested as it follows: a certain amount of this particle was used to absorb MO during 18 h from a solution containing more dye than the LDO can uptake to ensure a saturation state. Afterward, the concentration of MO in the solution is measured, and the saturated CCA500 is calcined at 500 °C for 4 h to decompose the organic matter. Then the recovered LDO was reused keeping the ratio of MO and adsorbent in every cycle. Four cycles were done.

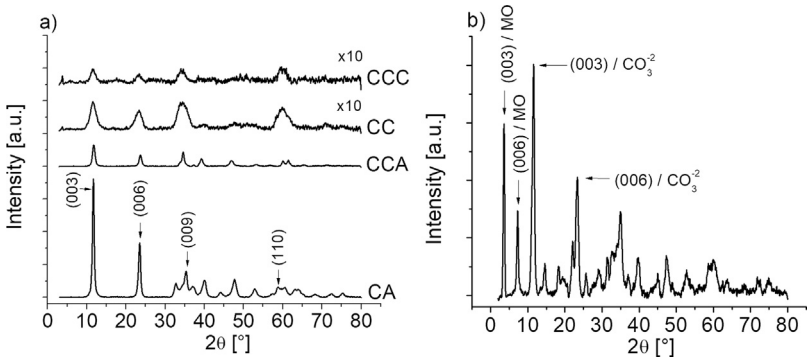

Fig. 1. X-ray diffractions from the different LDH samples studied: a) as-synthesized LDH and b) CA LDH after the methyl orange adsorption experiment.

Results and discussion

Fig. 1a shows the X-ray diffraction peaks associated with the different samples synthesized by our methodology. For layered double hydroxide compounds (LDH), the most relevant peaks appeared at low angles coming from well oriented and ordered supra-structure layers similar to hydrotalcite. In our samples, these peaks appeared at 11.7° and 23.4° meaning an interlayer distance around 22.6 Å. The intensity of these peaks depended on the particles analyzed with CA LDH (Cu/Al molar ratio of 5:2) presenting the highest diffraction intensities and therefore the highest crystallinity validating our method. By adding Co into the CA structure (CCA), the intensity of these peaks decreased showing that this ion disrupts the crystal and lamellae structure of the original LDH. Our co-precipitation method was not able to produce well-ordered CC LDH as the low angle diffraction intensities were drastically reduced as compared with CA and CCA samples, in addition to a bigger full width at half maximum intensity (FWHM), also related to a poor crystallinity [41,42]. Two Cu/Al ratios were further tested: 3:1 and 2:1, affecting the LDH crystallinity as evaluated by X-ray diffractions (results now shown). These results showed that the largest crystallinities of LDH were found at low Cu content due to the Jahn–Teller distortion of Cu^{2+} ion, leading to poor long-range ordering [37].

Scanning electron microscopy images (SEM) displayed in Fig. 2 confirmed the results from X-ray diffraction. For instance, CA LDH were characterized by layered particles of around 15 nm thickness and lateral sizes of around 150 nm (Fig. 2a). Despite the lower diffraction intensities of CCA LDH, as compared with CA, the morphologies of these particles were similar (Fig. 2b). CC samples presented a more amorphous structure, as concluded by X-ray diffraction, although layered structures dispersed through amorphous structures were also observed (Fig. 2c).

The chemical composition and morphology also affected the specific surface area of the LDH as summarized in Table 1. While CA and CCA LDH displayed values around 50 m^2/g that are currently found in this kind of layered structures [40], CC and CCC LDH displayed values as high as 140 m^2/g. The increased surface area in less crystalline LDH can be associated with the appearance of mesoporous from stacking defects [43]. Incomplete formation of the LDH layers can create a porosity associated with discontinuous layers at the interface producing necking of mesopores and open mesopores.

Table 1 further shows the results of the optical bandgap from the different samples measured by diffuse-reflectance UV–vis spectra based on the extrapolation of the Tauc/Davis–Mott expression. It is clear from this table the relevance of the LDH chemical composition on the bandgap as pure CA and CC LDH presented values of 3.7 and 2.4 eV, respectively. Therefore, by changing the M^{III} metal from Al^{3+} to Cr^{3+} the bandgap can be decreased. In a similar Cu/Cr LDH system with M^{II}/M^{III} ratio of 1.94, a value of 1.73 eV was reported although this sample presented a much higher crystallinity than our sample [44]. Different authors explained the energy transition change by processes associated with either metal-to-metal or ligand-to-metal charge transfer excitations from the MO_6 octahedral of the layered structure [13]. Although it has been reported that electron-transfer capability of cobalt can modify the band-gap, Table 1 shows that this transition was barely modified in our case [13].

The adsorption capacities of LDH were studied by Langmuir and Freundlich models allowing a proper quantification of this process. The adsorption capacity at equilibrium was calculated by [45]:

$$q_e = \frac{(C_0 - C_e)V}{m} \quad (1)$$

where C_0 is the initial concentration, C_e is the concentration at equilibrium (after being shaken for 24 h), V is the volume of the sample (in L), and m the mass of adsorbent used in the test (in g). From these concentrations of MO adsorbed the Langmuir isotherm in its linear form can be obtained [45]:

$$\frac{C_e}{q_e} = \frac{1}{q_m K_L} + \frac{C_e}{q_m} \quad (2)$$

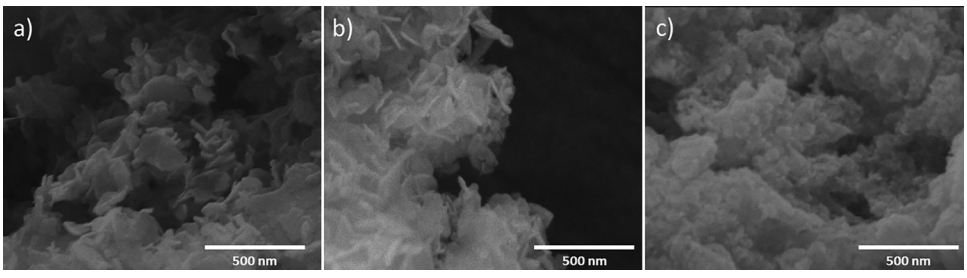

Fig. 2. Scanning electron microscopy images (SEM) of representative LDH particles: a) CA; b) CCA; and CC.

Table 1
Main properties of the different LDH and LDO samples prepared: a) bandgap as measured by diffuse-reflectance UV–vis spectra based on the extrapolation of the Tauc/Davis–Mott expression; b) q_m and K_L: maximum monolayer adsorption capacity and the constant from the Langmuir isotherm; c) n is the level depending on removal equilibrium concentration from the Freundlich equation; and d) specific surface area from BET analysis. Adsorption values were measured using methyl orange.

Sample	Bandgap [eV]	q_m [mg/g]	K_L [L/mg]	1/n	Specific area [m^2/g]
CA	3.70	LDH = 313	LDH = 0.03	LDH = 0.469	LDH = 42
		LDO = 780	LDO = 0.288	LDO = 0.17	LDO = 51
CCA	3.80	LDH = 243	LDH = 0.09	LDH = 0.420	LDH = 61
		LDO = 583	LDO = 0.482	LDO = 0.218	LDO = 65
CC	2.42	LDH = 107	LDH = 0.077	LDH = 0.508	LDH = 144
CCC	2.85	LDH = 61	LDH = 0.557	N/A	LDH = 134

where q_m is the maximum adsorption capacity (mg/g) and K_L is the Langmuir constant related to the energy of adsorption (L/mg). The Freundlich isotherm otherwise could be represented as:

$$q_e = K_F \cdot C_e^{1/n} \quad (3)$$

where n and K_F ($mg^{1-n} L^n$)/g) are Freundlich parameters, where n is the level depending on removal equilibrium concentration; and K_F is generally related to the adsorption ability of the adsorbent when the value of the adsorbate concentration is equal to 1. By performing isotherms at different LDH concentrations, the values reported in Table 1 were obtained. Examples of the Langmuir isotherm in its linear form (Eq. (2)) for CA and CCA LDH are displayed in Fig. 3a. The CA and CCC LDH displayed the highest MO adsorptions with values of 313 and 243 mg/g, respectively, meanwhile CC and CCC LDH displayed the lowest ones. Noteworthy, a relationship between the crystallinity of the sample and the adsorption can be concluded by comparing results from Table 1 and diffraction patterns from Fig. 1, as previously reported [46]. The values from this work's crystalline Cu/Al based LDH are comparable to previous results from other LDH having values around 300 mg/g for Congo red [28] and 443 mg/g for MO [27]. The latter being the highest value reported for MO compounds. The values reported here are not as high but were obtained from LDH materials produced by room temperature co-precipitation. These high adsorption values seem to relate not only with the crystallinity of LDH but also with its chemical compositions as there is a large effect of both the M^{2+}/M^{3+} ratio and the cations used on the structural and chemical characteristics of LDH. For instance, the smaller the difference of polarizing power between the divalent and the trivalent cations, the larger the composition ranges of the corresponding LDH [47]. Moreover, different combinations of cations can produce different environments and chemical affinities in the brucite-like layers allowing a large variety of anionic species together with water molecules to enter between the layers, affecting the adsorption process [48]. For instance, by comparing Ca/Al and Ni/Al LDH was concluded that the former particles presented higher total oxygen-containing functional groups providing more active sites for the binding of ions improving the adsorption efficiency [49].

The high adsorption process in LDH materials is related to hydrogen bonding between surface O—H groups from LDH and N or O atoms from MO meaning that MO molecules are bonded to the adsorbent surfaces [27]. However, electrostatic interaction, ion exchange, and surface complexation may also be considered [27]. Fig. 1b displays the diffraction pattern of CA LDH after the adsorption process showing that together with the (003) and (006) peaks from intercalated layers having the original carbonate molecules, new peaks at 3.6° and 7.2° appeared. MO^- molecules intercalated into LDH by exchanging CO_3^{2-} ions can increase the interlayer distances associated with the plane 003 [16]. The presence of interlayer distances associated with both MO^- and CO_3^{2-} counter-ions means that the anion exchange is not complete [16]. This confirms recent reports stating that the adsorption process in LDH is associated with two main phenomena: adsorption of anions on the external surface and anion exchange [50]. In the former process, the particle surface area plays a key role as also observed in other sorbents such as activated carbon. Recently, the relevance of the LDH surface characteristics on the adsorption process was confirmed during GO coagulation [24]. However, the second process involving anion exchange is unique for clay based materials such as LDH [51].

It is well known that calcination can increase the adsorption capacity of LDH by producing LDO [28]. Below 450 °C, LDH release surface and interstitial water and both carbon dioxide and water from dehydroxylation are produced. However, between 450–500 °C, calcined LDH lose their layer structure forming highly active composite metal oxides with high thermal stability, large surface area, basic properties, small crystal size, and high stability against sintering even under extreme conditions [40]. Therefore, CA, CCA, CC and CCC LDH were thermally treated at 500 °C for 4 h in

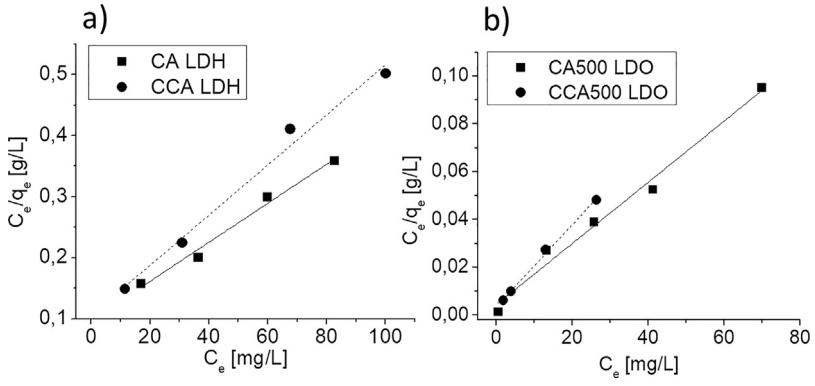

Fig. 3. Langmuir isotherms in its linear form (see Eq. (2)) for: a) CA and CCA LDH; and b) CA and CCA LDO samples.

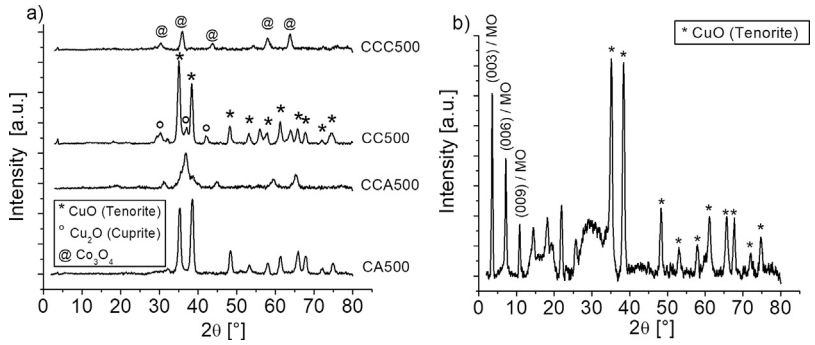

Fig. 4. X-ray diffractions from the different LDO samples studied: a) after LDH thermal treatment at 500 °C during 4 h; and b) CA500 LDO sample after MO adsorption test.

order to produce the corresponding LDO particles as confirmed by X-ray diffraction (Fig. 4a). CA and CC LDH after calcination displayed mainly copper oxide compounds such as tenorite and cuprite associated with the diffraction peaks at 35.2 and 38.4°, and 30.1, and 42.0°, respectively. Notably, the minor presence of Co in both CCA and CCC LDH disrupted the crystal phase of copper oxides favoring the appearance of crystals associated with Co_3O_4. Representative SEM images of the resulting LDO are displayed in Fig. 5 for CCA500 and CC500 LDO. Cu/Al based LDO presented a layered structure meanwhile Cu/Cr based LDO did not display any layered morphology, similar to the former LDH structures.

Table 1 displays the values of maximum adsorption capacity of the LDO coming from the most crystalline and layered LDH (CA500 and CCA500) confirming the large improvement by calcination. Examples of the Langmuir isotherm in its linear form (Eq. (2)) for CA and CCA LDO are displayed in Fig. 3b. Values as high as 780 and 583 mg/g were obtained for CA500 and CCA500, respectively, that cannot be explained by changes in specific areas as LDH and LDO presented similar values (see Table 1) [50]. To go further in the characterization of these particles, the N_2 adsorption isotherms from CA and CCA particles were analyzed (results not shown). CA and CCA LDH presented both a type II isotherm associated with a non-porous or macroporous adsorbent having unrestricted monolayer–multilayer adsorption and a H3 loop hysteresis related with the presence of aggregates of plate-like particles giving rise to slit-shaped pore in agreement with the LDH morphology [52]. These results further confirm that the addition to cobalt ions did not alter the layered morphology. Regarding the results from CA and CCA LDO, the hysteresis loop is similar to CA and CCA LDH meaning that layer structure was not affected by calcination as also confirmed by specific area values (see Table 1) and SEM images (Fig. 5). Moreover, there are not changes in pore volume and diameter between LDH and LDO. Therefore, the high adsorption of our LDO does not come from a complete loss of the layered structure, although some disruption can be concluded from X-ray diffractions associated with the disappearance of the peak at low angles.

The increased adsorption of LDO has been explained by the LDH reconstruction process by the intercalation of both organic molecules and $CO_3^{2-}/HCO_3^{-}/OH^{-}$ ions from water into the layered host structure, a process named "memory effect" [40]. The rehydration of mixed metal oxides and concurrent intercalation of oxyanions into the interlayer to reconstruct the LDH further explain this phenomenon. For LDH otherwise, the sorption process is primarily due to the ion exchange of the interlayer anions explaining their lower adsorption. To confirm this memory, or reconstruction effect, diffraction analysis was performed to the CA500 LDO sample after the adsorption process (Fig. 4b). This figure clearly shows that after adsorption new peaks associated with a layered morphology appeared meaning a reconstruction process by adsorption of MO. Notably, these peaks are at 3.7 and 7.1°, near to the values obtained in LDH after MO adsorption by ion exchange. Based on these findings we can confirm previous recent results regarding adsorption mechanisms. In both LDH and LDO there are some common processes regarding the interaction between metal ions from the layered particles (associated with metal–oxygen–metal and oxygen–metal–oxygen groups) and the $-SO_3^{-}$ groups of MO that suggests surface complexation and electrostatic interaction [53]. However, each particle also presents specific mechanisms as confirmed by our XRD results such as: ion exchange in LDH and "memory effect" in LDO.

The kinetics of adsorption is one of the most important characteristics that define the efficiency of adsorption describing the MO uptake rate governing the residence time of the adsorption reaction. CA LDH and CA500 LDH samples were selected for kinetic studies as observed in Fig. 6a showing that the adsorption is complete after around 40 min of contact for both particles. From the different kinetic models available, several studies confirm that

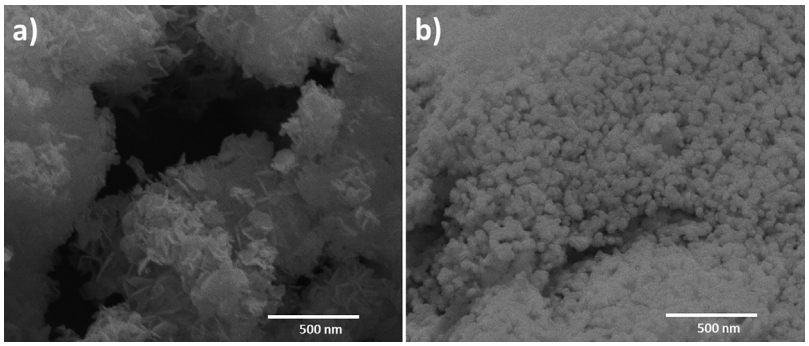

Fig. 5. Representative SEM images of the representative LDO samples: a) CCA500; and b) CC500.

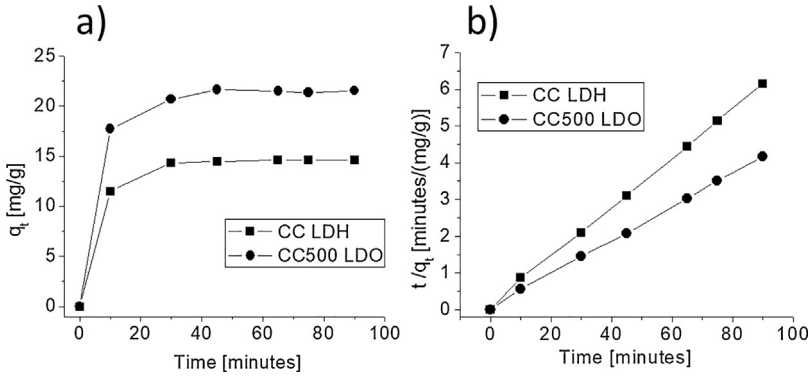

Fig. 6. Kinetics of adsorption for CC LDH and CC500 LDO: a) amount of MO (mg/g) adsorbed versus time t and b) linear form of a pseudo-second-order model (see Eq. (4)).

in these particles the results can be best fitted by a pseudo-second-order model that in its linear form is [28,50]:

$$\frac{t}{q_t} = \frac{1}{K_2 \cdot q_e^2} + \frac{t}{q_e} \quad (4)$$

where q_e and q_t are the amount of MO (mg/g) adsorbed at equilibrium and at time t, respectively; and K_2 is the rate constant (g/(mg min)). Fig. 6b shows the linear relationship obtained from this model with correlation coefficients (R^2) higher than 0.9992 confirming that this model is able to reproduce the experimental results. For CC LDH and CC500 LDO the values obtained for q_e are 14.8 and 21.8 mg/g, respectively meaning that calcination increase the adsorption capacity of the particle as concluded with the isotherm models. Noteworthy, the rate constant for CC LDH and CC500 LDO materials are 0.055 and 0.044 g/(mg min) meaning that the adsorption rate of MO onto the calcined product is slower than that onto LDH [50].

In order to evaluate potential applications for these LDO materials, the effect of different MO adsorption cycles was tested for the CCA500 sample (Fig. 7). A steady decrease in the adsorption capacity was observed reaching a plateau around 65% adsorption compared with the as synthesized sample after four cycles. This decrease is due to a considerable amount of degradation products from azo dyes not thermally decomposed at 500 °C blocking adsorption sites in the LDO [54].

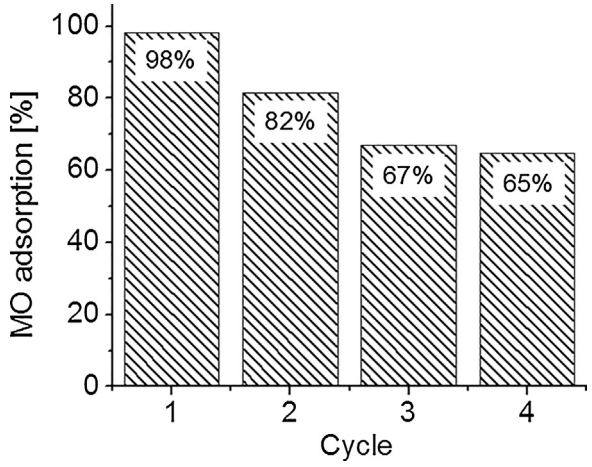

Fig. 7. Effect of different methyl orange (MO) adsorption cycles in CCA500 sample.

Conclusions

A simple room temperature co-precipitation method was developed allowing the synthesis of copper based LDH by using Al^{3+} and Cr^{3+} cations. Cu/Al based LDH presented crystalline layered structures meanwhile Cu/Cr based LDH displayed a more disorder state as confirmed by X-ray diffractions and SEM images. The addition of Co^{2+} anions decreased the crystallinity of the LDH by our method. Diffuse reflectance UV–vis spectroscopy showed that the band-gap transition of the different LDH was shifted depending on their chemical structures. A relationship between LDH crystallinity and MO adsorption was concluded with Cu based LDH presenting the highest maximum monolayer adsorption capacities: 313 and 240 mg/g, for pure Cu/Al and Cu/Co/Al respectively. By a calcination process producing LDO, these values increased to 780 and 583 mg/g, respectively. An adsorption mechanism based on ion exchange and reconstruction of the bilaminar structure was confirmed.

Acknowledgment

The authors gratefully acknowledge the financial support of CONICYT under FONDECYT project 1150130.

References

[1] N.E. Fard, R. Fazaeli, Int. J. Chem. Kinet. 48 (2016) 691.
[2] D. Robati, B. Mirza, M. Rajabi, O. Moradi, I. Tyagi, S. Agarwal, V.K. Gupta, Chem. Eng. J. 284 (2016) 687.
[3] A. Houas, H. Lachheb, M. Ksibi, E. Elaloui, C. Guillard, J. Herrmann, Appl. Catal. B: Environ. 31 (2001) 145.
[4] H. Lachheb, E. Puzenat, A. Houas, M. Ksibi, E. Elaloui, C. Guillard, J. Herrmann, Appl. Catal. B: Environ. 39 (2002) 75.
[5] B. Shah, A. Shah, P. Shah, Arch. Appl. Sci. 3 (2011) 327.
[6] Z. Yang, F. Wang, C. Zhang, G. Zeng, X. Tan, Z. Yu, Y. Zhong, H. Wang, F. Cui, RSC Adv. 6 (2016) 79415.
[7] D.G. Evans, R.C.T. Slade, Struct. Bond. 119 (2006) 1.
[8] Y. Zhao, X. Jia, G.I.N. Waterhouse, L.Z. Wu, C.H. Tung, D. O'Hare, T. Zhang, Adv. Energy Mater. 6 (2016) 1501974 (20 pages)..
[9] M. Shao, J. Han, M. Wei, D.G. Evans, X. Duan, Chem. Eng. J. 168 (2011) 519.
[10] P.R. Chowdhury, K.G. Bhattacharyya, Photochem. Photobiol. Sci. 16 (2017) 835.
[11] M. Lv, H. Liu, J. Solid State Chem. 227 (2015) 232.
[12] L. Tian, Y. Zhao, S. He, M. Wei, X. Duan, Chem. Eng. J. 184 (2012) 261.
[13] K. Parida, L. Mohapatra, N. Baliarsingh, J. Phys. Chem. C 116 (2012) 22417.
[14] S. Kim, J. Fahel, P. Durand, E. André, C. Carteret, Eur. J. Inorg. Chem. (2017) 669.
[15] S. Xia, X. Zhang, X. Zhou, Y. Menga, J. Xue, Z. Nia, Appl. Catal. B: Environ. 214 (2017) 78.
[16] G. Darmograi, B. Prelot, G. Layrac, D. Tichit, G. Martin-Gassin, F. Salles, J. Zajac, J. Phys. Chem. C 119 (2015) 23388.
[17] L. Lu, J. Li, D.H.L. Ng, P. Yang, P. Song, M. Zuo, J. Ind. Eng. Chem. 46 (2016) 315.
[18] L. Ai, C. Zhang, L. Meng, J. Chem. Eng. Data (2011) 4217.
[19] A. Guzmán-Vargas, E. Lima, G.A. Uriostegui-Ortega, M.A. Oliver-Tolentino, E.E. Rodríguez, Appl. Surf. Sci. 363 (2016) 372.
[20] T. Kameda, T. Uchiyama, T. Yoshioka, New J. Chem. 39 (2015) 6315.
[21] Y. Zou, X. Wang, Z. Chen, W. Yao, Y. Ai, Y. Liu, T. Hayat, A. Alsaedi, N.S. Alharbi, X. Wang, Environ. Pollut. 219 (2016) 107.

[22] Y. Zou, X. Wang, Y. Ai, Y. Liu, J. Li, Y. Ji, X. Wang, Environ. Sci. Technol. 50 (2016) 3658.
[23] X. Liu, J. Li, Y. Huang, X. Wang, X. Zhang, X. Wang, Environ. Sci. Technol. 51 (2017) 6156.
[24] J. Wang, Y. Li, W. Chen, J. Peng, J. Hua, Z. Chen, T. Wena, S. Lu, Y. Chen, T. Hayat, B. Ahmad, X. Wang, Chem. Eng. J. 309 (2017) 445.
[25] P. Kowalik, M. Konkol, M. Kondracka, W. Próchniak, R. Bicki, P. Wiercioch, Appl. Catal. A Gen. 464–465 (2013) 339.
[26] H. Zaghouane-Boudiaf, M. Boutahala, L. Arab, Chem. Eng. J. 187 (2012) 142.
[27] W. Yao, S. Yu, J. Wang, Y. Zou, S. Lu, Y. Ai, N.S. Alharbi, A. Alsaedi, T. Hayat, X. Wang, Chem. Eng. J. 307 (2017) 476.
[28] C. Lei, X. Zhu, B. Zhu, C. Jiang, Y. Le, J. Yu, J. Hazard. Mater. 321 (2017) 801.
[29] J. Barrault, A. Derouault, G. Courtois, J.M. Maissant, J.C. Dupin, C. Guimon, H. Martinez, E. Dumitriu, Appl. Catal. A Gen. 262 (2004) 43.
[30] R. Manivannan, A. Pandurangan, Appl. Clay Sci. 44 (2009) 137.
[31] I.C. Marcu, D. Tichit, F. Fajula, N. Tanchoux, Catal. Today 147 (2009) 231.
[32] S. Tanasoi, N. Tanchoux, A. Urdă, D. Tichit, I. Săndulescu, F. Fajula, I.C. Marcu, Appl. Catal. A Gen. 363 (2009) 135.
[33] J.S. Valente, J. Hernandez-Cortez, M.S. Cantu, G. Ferrat, E. López-Salinas, Catal. Today 150 (2010) 340.
[34] L.H. Zhang, F. Li, D.G. Evans, X. Duan, J. Mater. Sci. 45 (2010) 3741.
[35] M. Turco, G. Bagnasco, U. Costantino, F. Marmottini, T. Montanari, G. Ramis, G. Busca, J. Catal. 228 (2004) 43.
[36] M. Behrens, I. Kasatkin, S. Kühl, G. Weinberg, Chem. Mater. 22 (2010) 386.
[37] S. Li, H. Wang, W. Li, X. Wu, W. Tanga, Y. Chen, Appl. Catal. B: Environ. 166–167 (2015) 260.
[38] H. Palza, N. Saldias, P. Arriagada, P. Palma, J. Sanchez, JOM 69 (2017) 1319.
[39] X. Long, Z. Wang, S. Xiao, Y. An, S. Yang, Mater. Today 19 (2016) 213.
[40] K.H. Goh, T.T. Lim, Z. Dong, Water Res. 42 (2008) 1343.
[41] U. Costantino, F. Marmottini, M. Nocchetti, R. Vivani, Eur. J. Inorg. Chem. 1998 (1998) 1439.
[42] T.P.F. Teixeira, S.F. Aquino, S.I. Pereira, A. Dias, Braz. J. Chem. Eng. 31 (2014) 19.
[43] S.K. Yun, T.J. Pinnavaia, Chem. Mater. (1995) 348.
[44] N. Baliarsingh, K.M. Parida, G.C. Pradhan, Ind. Eng. Chem. Res. 53 (2014) 3834.
[45] X. Ruan, Y. Chen, H. Chen, G. Qian, R.L. Frost, Chem. Eng. J. 297 (2016) 295.
[46] K.H. Goh, T.T. Lim, Z. Dong, Water Res. 42 (2008) 1343.
[47] B. Gregoire, C. Ruby, C. Carteret, Cryst. Growth Des. 12 (2012) 4324.
[48] M. Al-Jaberi, S. Naille, M. Dossot, C. Ruby, J. Mol. Struct. 1102 (2015) 253.
[49] Y. Zou, Y. Liu, X. Wang, G. Sheng, S. Wang, Y. Ai, Y. Ji, Y. Liu, T. Hayat, X. Wang, ACS Sustain. Chem. Eng. 5 (2017) 3583.
[50] B. Li, Y. Zhang, X. Zhou, Z. Liu, Q. Liu, X. Li, J. Alloys Compd. 673 (2016) 265.
[51] J. Orthman, H.Y. Zhu, G.Q. Lu, Sep. Purif. Technol. 31 (2003) 53.
[52] K.S.W. Sing, D.H. Everett, R.A.W. Haul, L. Moscou, R.A. Pierotti, J. Rouquerol, T. Siemieniewska, Pure Appl. Chem. 57 (1985) 603.
[53] W. Yao, S. Yu, J. Wang, Y. Zou, S. Lu, Y. Ai, N.S. Alharbi, A. Alsaedi, T. Hayat, X. Wanga, Chem. Eng. J. 307 (2017) 476.
[54] T.P.F. Teixeira, S.F. Aquino, S.I. Pereira, A. Dias, Braz. J. Chem. Eng. 31 (2014) 19.